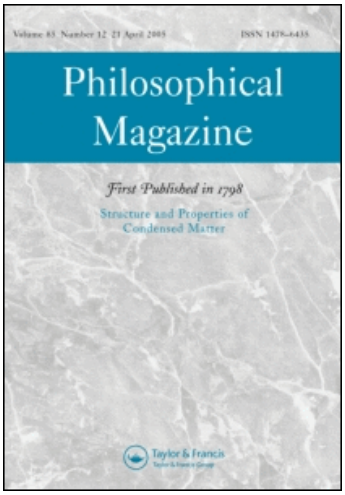

Philosophical Magazine
Publication details, including instructions for authors and subscription information:
http://www.informaworld.com/smpp/title~content=t713695589

Orbital-free density functional theory simulations of dislocations in aluminum

Ilgyou Shin [a]; Ashwin Ramasubramaniam [b]; Chen Huang [c]; Linda Hung [b]; Emily A. Carter [bd]
[a] Department of Chemistry, [b] Program in Applied and Computational Mathematics, [c] Department of Physics, [d] Department of Mechanical and Aerospace Engineering, Princeton University, Princeton, NJ 08544-5263, USA

Online publication date: 01 December 2009

To cite this Article Shin, Ilgyou, Ramasubramaniam, Ashwin, Huang, Chen, Hung, Linda and Carter, Emily A.(2009) 'Orbital-free density functional theory simulations of dislocations in aluminum', Philosophical Magazine, 89: 34, 3195 — 3213
To link to this Article: DOI: 10.1080/14786430903246353
URL: http://dx.doi.org/10.1080/14786430903246353

Philosophical Magazine
Vol. 89, Nos. 34–36, 1–21 December 2009, 3195–3213

Taylor & Francis
Taylor & Francis Group

Orbital-free density functional theory simulations of dislocations in aluminum

Ilgyou Shin[a], Ashwin Ramasubramaniam[b], Chen Huang[c], Linda Hung[b] and Emily A. Carter[bd]*

[a]*Department of Chemistry;* [b]*Program in Applied and Computational Mathematics;* [c]*Department of Physics and* [d]*Department of Mechanical and Aerospace Engineering, Princeton University, Princeton, NJ 08544-5263, USA*

(*Received 28 May 2009; final version received 5 August 2009*)

The core structure of screw and edge dislocations in fcc Al was investigated using orbital-free density functional theory (OF-DFT). Detailed calibrations of kinetic energy density functionals (KEDFs) and local pseudopotentials were performed to reproduce accurately the energies of several phases of bulk Al, as well as the elastic moduli and stacking fault energies of fcc Al. Thereafter, dislocations were modeled with both periodic and non-periodic cells containing a few thousand atoms, and the widths of the dissociated cores were extracted. The results are in good agreement with previous estimates from experiment and theory, further validating OF-DFT with non-local KEDFs as a seamless and accurate tool for simulating large features in main group, nearly-free-electron-like metals at the mesoscale.

Keywords: aluminum; computer simulation; defects in solids; density functional theory; dislocations

1. Introduction

Computer simulations have steadily evolved over the last few decades to be an indispensable tool for probing materials behavior. The ability to glean information at atomic scales from computer experiments has significantly advanced our understanding of fundamental mechanisms that govern the overall macroscopic behavior of materials [1,2]. The sustained increase in computational power, combined with the development of efficient algorithms, has enabled simulations of systems containing several hundreds to millions of atoms, the attainable system size being a function of the level of theory used to describe the material (e.g. quantum mechanics, classical potentials, etc.). Among various quantum mechanical methods, Kohn–Sham density functional theory (KS-DFT) [3,4] has found widespread application and success in materials modeling, which may be attributed to a reasonable balance between accuracy and computational cost. Nevertheless, even with this

*Corresponding author. Email: eac@princeton.edu

ISSN 1478–6435 print/ISSN 1478–6443 online

DOI: 10.1080/14786430903246353
http://www.informaworld.com

moderate computational cost, routine calculations on thousands of atoms are not yet possible with KS-DFT [5–10], despite the fact that the traditional cubic scaling of KS-DFT can be made linear for non-metals [11–15]. Therefore, interatomic potential methods have remained the tool of choice for simulating large atomistic systems despite being less accurate than KS-DFT.

Among several extant formulations of interatomic potentials, metallic systems are generally described accurately by potentials that capture the many-body aspects of metallic bonding. In particular, the Finnis–Sinclair model [16], rooted in the second-moment approximation to the tight-binding model, and the embedded atom method (EAM) [17,18], formally based on DFT, have found widespread success in simulations of simple metals and intermetallics. The functional forms for the interatomic potentials employed in these approaches are amenable to rapid evaluation, yet are sufficiently flexible to allow for parameterization over a wide range of equilibrium and non-equilibrium properties. Although the very formulation of these potentials renders them less accurate when bonds have strong directionality (e.g. in covalent solids, metals with partially filled *d*-shells), a larger drawback is the frequent lack of transferability to environments that differ significantly from those in which the potential was originally fit. Furthermore, developing potentials for alloys involves additional functions that must be fit for the cross-interaction of different species, beyond the mere development of elemental potentials for its constituents. The additional effort and complexity required has inhibited the extension of such methods to complex alloys. This stands in stark contrast to DFT, which, in principle, requires as sole input the atomic numbers (or pseudopotentials) of the various species present in a simulation. Therefore, the development of simulation tools that afford the versatility and accuracy of KS-DFT with the ability to simulate moderately large system sizes, similar to interatomic potential methods, remains an active area of research.

The orbital-free density functional theory (OF-DFT) method is a first-principles quantum mechanical method that is comparable in accuracy to KS-DFT for main group, nearly-free-electron-like metals and yet is significantly less computationally expensive [19–23]. Unlike KS-DFT, which uses one-electron orbitals to evaluate the non-interacting electron kinetic energy, OF-DFT relies on the electron density as the sole variable in the spirit of the first Hohenberg–Kohn theorem [3]. The absence of one-electron orbitals eliminates the overhead of k-point sampling of the Brillouin zone, a technique which significantly increases the computational cost of KS-DFT, especially for metallic systems. Furthermore, the electronic terms in OF-DFT can be made to scale nearly linearly [$O(N \ln N)$] using fast Fourier transforms [24], as can the ionic (screened nuclei) terms in OF-DFT, by means of spline interpolation of the structure factor [25–28]. The accuracy of OF-DFT depends significantly upon the accuracy of the kinetic energy density functional (KEDF), employed in lieu of the KS-DFT kinetic energy expression. State-of-the-art KEDFs are based on the linear response of a uniform electron gas [29–32]. Hence, the applicability of OF-DFT is limited at present to main group, nearly-free-electron-like metals. However, unlike the EAM or Finnis–Sinclair approaches, which employ (or assume) a frozen-density approximation, the electron density is optimized through self-consistent iterations in OF-DFT. This density relaxation procedure naturally endows OF-DFT with greater accuracy and transferability. Of course, the computational overhead

associated with self-consistency cycles makes OF-DFT more expensive than classical potential methods.

In this work, we employ OF-DFT simulations to study dislocations in Al, a nearly-free-electron-like metal. Dislocations, the carriers of plasticity, play a central role in the strength of metals. Accurate modeling of the structure of dislocations, their mutual interaction, as well as their interaction with external stress fields and internal lattice defects, is crucial for understanding the mechanical behavior of metals and for guiding the design of improved structural materials. In face-centered-cubic (fcc) metals, perfect $\langle 110\rangle/\{111\}$ dislocations typically dissociate into two $\langle 112\rangle/\{111\}$ Shockley partials that bound a stacking fault region, which is locally hexagonal-close-packed (hcp) [33]. The spacing between these partials (the dislocation width) is largely determined by the stacking fault energy (SFE) and can be estimated using standard linear elasticity methods [33]. However, for materials such as Al, which have relatively large stacking fault energies, the dislocation spacing becomes sufficiently small that interactions between the partial dislocation cores become significant enough to necessitate a more detailed atomistic analysis. Measurements from weak-beam transmission electron microscopy [34] indicate typical edge dislocation widths of 8 Å. High-resolution transmission electron microscopy studies [35,36] indicate average dislocation widths of 40 Å; it should be emphasized that those studies examined deformed nanocrystalline samples in which the effects of internal stresses could be significant. EAM simulations give a range of 5–15 Å as typical dislocation widths [37,38]. While direct KS-DFT simulations of dislocations are still too expensive, multiscale/multiphysics methods such as the first-principles lattice Green function boundary condition (FP-GFBC) method [39,40] and the quasi-continuum DFT (QC-DFT) [41] technique have been employed to study dislocation cores in Al. The common feature of these techniques is the coupling of a full quantum mechanical treatment (KS-DFT) of a subset of atoms at the dislocation core with a more approximate level of theory (EAM/lattice Green functions) further away from the core. As is invariably the case with such methods, great care must be exercised in ensuring error-free coupling, both mechanical (forces) and electronic (charge density), at various interfaces in the simulation. FP-GFBC studies [40] report widths of 5.0–7.5 Å and 7.0–9.5 Å for screw and edge dislocations, respectively, while QC-DFT studies [41] report a width of 5.6 Å for edge dislocations in Al. In both studies, roughly 100 atoms were treated with KS-DFT, which raises some concern regarding the accuracy of the core structure. OF-DFT allows for direct simulation of the core structure of dislocations and their immediate surroundings with first-principles accuracy combined with the ease of classical potential methods. In the following, we will apply this methodology to study core structures of screw and edge dislocations as well as the energetics of various stacking faults in fcc Al. Prior OF-DFT studies [20–22,29,30,42] have already demonstrated the accuracy and efficacy of OF-DFT in treating Al.

The organization of this paper is as follows. In Section 2, we outline the linear-scaling OF-DFT method with emphasis upon its main sources of potential error, namely the KEDF and the local pseudopotential. In Section 3, we provide computational details. In Section 4, we present OF-DFT predictions of elastic moduli, stacking faults, and dislocation cores in fcc Al. In particular, we examine the sensitivity of our results with respect to the KEDF, the exchange-correlation

functional, and the boundary conditions. Concluding remarks are provided in Section 5.

2. OF-DFT overview

The first Hohenberg–Kohn theorem proves that all ground state properties of a non-degenerate system are determined solely by the electron density. As a result, the total energy functional can be written as

$$E_{\mathrm{Tot}}[\rho] = E_{ii}(\vec{r}) + T_S[\rho] + E_{\mathrm{Hart}}[\rho] + E_{XC}[\rho] + \int V_{\mathrm{Ext}}(\vec{r})\rho(\vec{r})\mathrm{d}\vec{r}, \tag{1}$$

under the constraint that the electron density ρ is properly normalized to N, the number of electrons in the system, and is everywhere non-negative. In the above expression, $E_{ii}(\vec{r})$ is the ion–ion repulsion energy (where "ion" either refers to a bare nucleus or a nucleus screened by the core electrons), $T_S[\rho]$ is the kinetic energy of the non-interacting electrons, $E_{\mathrm{Hart}}[\rho]$ is the classical Hartree electron–electron repulsion energy, $E_{XC}[\rho]$ is the electron exchange-correlation energy (which also corrects for the kinetic energy of interacting electrons), and $V_{\mathrm{Ext}}(\vec{r})$ is the external potential (typically the electron–ion interaction potential, usually given as a pseudopotential). In our code, $E_{ii}(\vec{r})$ is computed using the particle-mesh Ewald method, which scales as $O(M \ln M)$ where M is the number of ions in the simulation cell [27]. $E_{\mathrm{Hart}}[\rho]$ and $E_{XC}[\rho]$ are computed in Fourier and real space, respectively, as described in [24]. Local pseudopotentials are used in OF-DFT to construct the external potential $V_{\mathrm{Ext}}(\vec{r})$, as described in Section 2.2. Next we describe how $T_S[\rho]$ is evaluated.

2.1. *Kinetic energy density functional*

The exact form of the KEDF is not known except in certain limits. Currently, the most accurate functionals available are the Wang–Govind–Carter (WGC) [29,30] and Wang–Teter (WT) [31] KEDFs, both designed to reproduce the Lindhard linear response of a free-electron gas [43]. These KEDFs consist of the Thomas–Fermi (TF) functional [44–46], the von Weizsäcker (vW) functional [47], and a linear response term. The TF KEDF, which is only exact for a uniform electron gas, has the form

$$T_{TF}[\rho] = C_{TF}\int_{\Omega} \rho(\vec{r})^{5/3}\mathrm{d}\vec{r}, \tag{2}$$

where $C_{TF} = \frac{3}{10}(3\pi^2)^{2/3}$. Use of the TF KEDF fails to reproduce shell structure for atoms and molecular binding [48,49], as the densities of atoms and molecules are far from uniform. The vW KEDF, which is only exact for a single orbital system (i.e. a bosonic ground state or a one-electron or two-electron-singlet ground state), has the form

$$T_{vW}[\rho] = \frac{1}{8}\int_{\Omega} \frac{\left|\nabla\rho(\vec{r})\right|^2}{\rho(\vec{r})}\mathrm{d}\vec{r}. \tag{3}$$

Neither the TF KEDF nor the vW KEDF, or even their linear combinations, reproduce the correct linear response behavior of a uniform electron gas, first derived analytically by Lindhard [43]. For a KEDF to obey Lindhard linear response, the following equation must hold:

$$\hat{F}\left(\left.\frac{\delta^2 T_S[\rho]}{\delta\rho(\vec{r})\delta\rho(\vec{r}')}\right|_{\rho_0}\right) = -\frac{1}{\chi_{\text{Lind}}}, \tag{4}$$

where ρ_0 is the average electron density, $\hat{F}[\cdot]$ denotes the Fourier transform and χ_{Lind} is the Lindhard susceptibility function in reciprocal space given by

$$\chi_{\text{Lind}} = -\frac{k_F}{\pi^2}\left(\frac{1}{2} + \frac{1-|\vec{\eta}|^2}{4|\vec{\eta}|}\ln\left|\frac{1+|\vec{\eta}|}{1-|\vec{\eta}|}\right|\right), \tag{5}$$

in reduced units, where $k_F = (3\pi^2\rho_0)^{1/3}$ is the Fermi wavevector and $\vec{\eta} = \vec{q}/2k_F$ is a dimensionless momentum.

To correctly reproduce the Lindhard response, Wang and Teter [31] introduced a third term in the KEDF that explicitly enforces this behavior. The resulting WT KEDF has the form

$$T_S^{\alpha,\beta}[\rho] = T_{TF}[\rho] + T_{vW}[\rho] + T_{WT}^{\alpha,\beta}[\rho], \tag{6}$$

where

$$T_{WT}^{\alpha,\beta}[\rho] = C_{TF}\int\int \mathrm{d}r^3\mathrm{d}r'^3\rho^{\alpha}(\vec{r})w_{\alpha,\beta}(\vec{r}-\vec{r}')\rho^{\beta}(\vec{r}'), \tag{7}$$

and the WT linear response kernel $w_{\alpha,\beta}(\vec{r}-\vec{r}')$ must satisfy the condition

$$\hat{F}[w_{\alpha,\beta}(\vec{r}-\vec{r}')] \equiv \tilde{w}_{\alpha,\beta}(\vec{q}) = -\frac{\chi_{\text{Lind}}^{-1} - \chi_{vW}^{-1} - \chi_{TF}^{-1}}{2\alpha\beta C_{TF}\rho_0^{\alpha+\beta-2}}. \tag{8}$$

In the above expression, $\chi_{TF} = -k_F/\pi^2$ and $\chi_{vW} = \chi_{TF}/3\eta^2$ are the response functions of the TF and vW KEDFs, respectively. The exponents α and β can either be treated as fitting parameters [23,31,32,50–54] or be determined from an asymptotic analysis [55,56].

In order to improve upon the WT KEDF, where the linear response kernel $w_{\alpha,\beta}(\vec{r}-\vec{r}')$ is dependent only on one value of the density ρ_0, Wang et al. [29,30] replaced the density-independent kernel of the WT KEDF with an explicit non-local, density-dependent kernel. Their KEDF has the form

$$T_S^{\alpha,\beta,\gamma}[\rho] = T_{TF}[\rho] + T_{vW}[\rho] + T_{WGC}^{\alpha,\beta,\gamma}[\rho], \tag{9}$$

where

$$T_{WGC}^{\alpha,\beta,\gamma}[\rho] = C_{TF}\int\int \mathrm{d}r^3\mathrm{d}r'^3\rho^{\alpha}(\vec{r})w_{\alpha,\beta}(\xi_\gamma(\vec{r},\vec{r}')|\vec{r}-\vec{r}'|)\rho^{\beta}(\vec{r}'), \tag{10}$$

and $\xi_\gamma(\vec{r},\vec{r}') = \left(\frac{k_F^\gamma(\vec{r})+k_F^\gamma(\vec{r}')}{2}\right)^{1/\gamma}$ and $k_F(\vec{r}) = [3\pi^2\rho(\vec{r})]^{1/3}$ are the non-local two-body and local one-body Fermi wavevectors, respectively. The WGC KEDF kernel $w_{\alpha,\beta}\left(\xi_\gamma\left(\overrightarrow{r},\overrightarrow{r}'\right)|\overrightarrow{r}-\overrightarrow{r}'|\right)$ is determined by solving a second-order differential

equation as discussed in [29,30] and [57]. The WGC exponents, $\alpha, \beta = \frac{5}{6} \pm \frac{\sqrt{5}}{6}$, are determined by asymptotic analysis [55,56], whereas γ is a material-specific adjustable parameter. For example, $\gamma = 2.7$ is found to be optimal for Al [29,30].

Since the WGC KEDF kernel is density-dependent, computation of the exact convolution scales quadratically. However, quasilinear scaling is achieved in practice by performing a Taylor series expansion of the WGC KEDF kernel, which factors out the density dependence in the kernel. The resulting kernel takes the form

$$\begin{aligned} w_{\alpha,\beta}(\xi_\gamma(\vec{r},\vec{r}')|\vec{r}-\vec{r}'|) = {} & w_{\alpha,\beta}(k_F^*|\vec{r}-\vec{r}'|) \\ & + \left.\frac{\partial w_{\alpha,\beta}(\xi_\gamma(\vec{r},\vec{r}')|\vec{r}-\vec{r}'|)}{\partial\rho(\vec{r})}\right|_{\rho_*}\theta(\vec{r}) + \left.\frac{\partial w_{\alpha,\beta}(\xi_\gamma(\vec{r},\vec{r}')|\vec{r}-\vec{r}'|)}{\partial\rho(\vec{r}')}\right|_{\rho_*}\theta(\vec{r}') \\ & + \left.\frac{\partial^2 w_{\alpha,\beta}(\xi_\gamma(\vec{r},\vec{r}')|\vec{r}-\vec{r}'|)}{\partial\rho^2(\vec{r})}\right|_{\rho_*}\frac{\theta^2(\vec{r})}{2} + \left.\frac{\partial^2 w_{\alpha,\beta}(\xi_\gamma(\vec{r},\vec{r}')|\vec{r}-\vec{r}'|)}{\partial\rho^2(\vec{r}')}\right|_{\rho_*}\frac{\theta^2(\vec{r}')}{2} \\ & + \left.\frac{\partial^2 w_{\alpha,\beta}(\xi_\gamma(\vec{r},\vec{r}')|\vec{r}-\vec{r}'|)}{\partial\rho(\vec{r})\partial\rho(\vec{r}')}\right|_{\rho_*}\theta(\vec{r})\theta(\vec{r}') + \cdots, \end{aligned} \tag{11}$$

where $\theta(\vec{r}) = \rho(\vec{r}) - \rho_*$, $k_F^* = (3\pi^2\rho_*)^{1/3}$, and ρ_* is a reference density, usually chosen to be average density ρ_0 of the system. Since the third derivative of $\tilde{w}$ involves the first derivative of the Lindhard function [57], which has a logarithmic discontinuity at $\eta = 1$, the Taylor series expansion can only be evaluated up to second order. In the work that follows, both WT and WGC KEDFs will be employed to provide points of comparison.

2.2. *Ion–electron energy*

Within KS-DFT, the interaction of valence electrons with the core electrons and nuclei is typically represented via non-local pseudopotentials (NLPS), which explicitly account for angular momentum dependence via orbital-based projection operators. Unfortunately, without orbitals there is no way to use angular-momentum-based pseudopotentials in OF-DFT, and therefore only radially-symmetric local pseudopotentials (LPSs) that depend solely upon the distance of the electron from the nucleus can be used. Recently, Zhou et al. [58] developed a new scheme to generate transferable LPSs derived from bulk crystalline densities by inverting the KS equations. They showed that a bulk-derived LPS (BLPS) for Si could reproduce NLPS predictions within KS-DFT. A weakness of this original BLPS construction is that a large kinetic energy cutoff is essential to achieve convergence with respect to the plane wave basis. More recently, Huang and Carter [42] modified Zhou et al.'s approach and developed much softer BLPSs by introducing a cutoff function, which eliminates oscillating tails in reciprocal space and real space. Since a softer BLPS allows for a lower kinetic energy cutoff for the plane wave basis expansion of the electron density, this further improves the computational efficiency of OF-DFT calculations. In this work, we employ Huang and Carter's BLPS for Al.

3. Computational details

All OF-DFT calculations are performed using PROFESS (PRinceton Orbital-Free Electronic Structure Software) which is a FORTRAN90 based program developed

by Carter and coworkers [24,25]. For purposes of comparison, KS-DFT calculations for phase orderings, elastic constants, and SFEs of Al are performed using the ABINIT software [59]. Both programs use a plane wave basis set. For describing electron exchange and correlation in KS- and OF-DFT, we use the local density approximation (LDA) derived from the Quantum Monte Carlo results of Ceperley and Alder [60] as parameterized by Perdew and Zunger [61] and the generalized gradient approximation (GGA) of Perdew, Burke and Ernzerhof (PBE) [62].

In OF-DFT calculations, we use both the WGC and WT KEDFs for purposes of comparison, with exponents $\alpha, \beta = \frac{5}{6} \pm \frac{\sqrt{5}}{6}$ in Equations (7) and (10); the parameter γ is set to a value of 2.7 in Equation (10). For ion–electron terms in OF-DFT, we use an LDA-based Al BLPS developed by Huang and Carter [42] for the LDA calculations and a corresponding GGA-based one constructed within the same scheme for the GGA calculations. These pseudopotentials are only fit to the KS-DFT energy ordering of a few Al phases (no experimental information is used) yet are found to reproduce accurately the corresponding results obtained with the Troullier–Martins (TM) NLPS [63]. The latter NLPSs are used to obtain the KS-DFT benchmarks in this work.

Since one of the exponents α, β $\left(\alpha, \beta = \frac{5}{6} \pm \frac{\sqrt{5}}{6}\right)$ in the non-local term of the WGC KEDF is smaller than 0.5, the corresponding potential $(= \delta T_{WGC}^{\alpha,\beta,\gamma}[\rho]/\delta\sqrt{\rho(\vec{r})})$ used in the electron density optimization step [24] may diverge in very low density (vacuum) regions and cause convergence problems. In order to keep using these values of α, β, which were formally derived from asymptotic analysis of the KEDF [55,56], we multiply this portion of the WGC KEDF potential by a smooth cutoff function to suppress its divergence in very low density regions. The cutoff function is

$$f(r) = \frac{e^{\rho(r)/D} - 1}{e^{\rho(r)/D} + e^{\rho_C/D}}, \tag{12}$$

where ρ_C is the density below which $f(r)$ goes to zero quickly and above which $f(r)$ approaches unity quickly. D controls the smoothness of this function at ρ_C, and we set $D = \rho_C/10$ in our PROFESS code. With ρ_C set to 10^{-5}, surface energies are affected by less than $1\,\mathrm{mJ\,m^{-2}}$, compared to no cutoff function. Indeed, very low-density regions should contribute negligibly to total DFT energies by definition. Thus, use of this cutoff function simply removes numerical instabilities due to the presence of vacuum while leaving the physics unchanged.

The numerical parameters of k-point meshes in KS-DFT and plane wave basis kinetic energy cutoffs in both KS- and OF-DFT are set to ensure convergence of total energies to 2.7×10^{-5} eV/atom (this stringent value is necessary when computing systems containing thousands of atoms to ensure that meaningful energy differences can be computed). In the KS-DFT calculations for elastic constants and minimum energies of various phases, we use a kinetic energy cutoff of 800 eV, a smearing width of 0.1 eV within a Fermi–Dirac smearing of the Fermi surface, a $20 \times 20 \times 20$ k-point mesh for simple cubic (sc), body-centred cubic (bcc) and fcc structures, and a $12 \times 12 \times 12$ mesh for hcp and diamond (dia) structures. For KS-DFT SFE calculations, we use a kinetic energy cutoff of 480 eV, a smearing

width of 0.1 eV, and a $10 \times 10 \times 1$ k-point mesh. We use the Broyden–Fletcher–Goldfarb–Shanno (BFGS) minimization, modified to account for the total energy as well as the gradients, for ion optimization in KS-DFT [59]. In the OF-DFT calculations for minimum energies of various phases, elastic constants, and SFEs, we use a larger kinetic energy cutoff of 1200 eV, since this kinetic energy cutoff is meant to converge the density rather than the orbitals. For the OF-DFT geometry optimization of dislocations, we use a 600 eV cutoff for initial optimization and then re-optimize the resulting structure with a 1200 eV cutoff. We use the truncated Newton method [64] for density optimization and the conjugate gradient method [65] for ion relaxation in OF-DFT. In all calculations, the convergence threshold for the maximum force component on any atom is 2.57×10^{-3} eV Å^{-1}.

Elastic constants are computed by applying homogeneous uniaxial, shear and hydrostatic strains to the optimized fcc bulk Al structure, and performing a quadratic fit to the energy versus strain curve. SFEs in bulk Al are calculated using the simulation cell and the procedure of Bernstein and Tadmor [66]. Studies of dislocation core structures are performed using both nilpotent arrangements of dislocations within fully periodic simulation cells [67] as well as single dislocations in cylindrical simulation cells. In the latter case, 20 Å of vacuum is employed between nearest neighbor dislocations in periodic supercells to eliminate artificial coupling between images; also, a region of atoms 5 Å in thickness at the surface of the cylinder is held fixed during relaxation (to impose the correct far-field displacement boundary condition on the dislocation). For the fully periodic calculations, we use an equi-spaced quadrupolar array of screw dislocations in an orthogonal cell. Edge dislocations, which require more atoms in the simulation cell (to eliminate recombination of oppositely signed dislocations), are simulated using a dipolar arrangement in a non-orthogonal cell, which results in a smaller number of atoms. Details of the various simulation cells used in this work are provided in Table 1; the cell sizes given therein are large enough that the interaction between dislocations is minimal (i.e. the dislocation widths are converged with respect to cell size; smaller cell sizes led to either recombination or spurious attraction between partial dislocations belonging to different dislocations in the quadrupole).

Table 1. Details of various supercells used in dislocation simulations. For both quadrupolar and isolated screw dislocations, the edges of the supercell are oriented along the $[1\bar{1}2]$, $[1\bar{1}\bar{1}]$ and [110] directions. For the edge dipole, the cell vectors are oriented along e_1, $\frac{1}{2}e_1 + \frac{1}{2}e_2$ and e_3, where e_1, e_2, and e_3 are unit vectors along the [110], $[1\bar{1}1]$ and $[\bar{1}12]$ directions. For the isolated edge dislocation, the axes of the supercell are oriented along the [110], $[1\bar{1}1]$ and $[\bar{1}12]$ directions.

Dislocation	Supercell	Number of atoms	Cell size (Å)
Screw	Quadrupole	2304	$119.0 \times 112.2 \times 2.863$
	Isolated single core	1332	$119.2 \times 119.2 \times 2.863$
Edge	Dipole	4320	$171.8 \times 120.2 \times 4.959$
	Isolated single core	3068	$134.5 \times 134.5 \times 4.959$

4. Results and discussion

4.1. *OF-DFT validation*

As an important method validation step, we first compare minimum energies of various phases of Al obtained from OF-DFT and KS-DFT calculations with various XC functionals and KEDFs, as shown in Table 2. First, by comparing KS-DFT/BLPS with KS-DFT/TM-NLPS results, we see that LDA- and GGA-based BLPSs accurately reproduce the TM-NLPS energies of bulk phases of Al, the errors being consistent with those of numerical and physical approximations in the model (i.e. less than 20 meV/atom, except for the LDA calculation of the sc structure). Even though the hcp structure was not used in the fitting procedure, the BLPSs accurately reproduce the small energy difference (<40 meV) between fcc and hcp structures obtained by TM-NLPS. Having ascertained the accuracy of the BLPSs, we will henceforth benchmark all OF-DFT results (which we recall can only employ BLPSs) against KS-DFT/BLPS. Upon comparing OF-DFT/BLPS to KS-DFT/BLPS (Table 2), we see that the agreement is excellent (errors less than 20 meV/atom) for all structures with the exception of the sc and dia structures. Lower accuracy can be expected for the sc and dia structures, since the WGC and WT KEDFs in OF-DFT are based on the linear response behavior of a uniform electron gas so that OF-DFT works better for close-packed structures, in which the electron density is distributed more evenly, closer to the uniform electron gas. Overall, the WGC KEDF is seen to be somewhat more accurate than the WT KEDF.

Next, we compare elastic constants and SFEs obtained from OF-DFT and KS-DFT. Within elasticity theory, the width of a dislocation is determined by the balance of the repulsive force between partials, which is proportional to the shear modulus, and the attractive force between partials, which is proportional to the SFE. Therefore, any estimate of dislocation core structure is predicated upon the accuracy

Table 2. KS-DFT and OF-DFT calculations for equilibrium total energies (eV/atom) of Al using TM-NLPS/BLPSs, WGC/WT KEDFs within OF-DFT, and LDA/GGA XCs. The equilibrium total energy of fcc Al is tabulated; for all other structures, the energy relative to the fcc structure is given. Results from GGA calculations are shown in parentheses. KS-DFT/TM-NLPS/LDA, KS-DFT/BLPS/LDA and OF-DFT/WGC/BLPS/LDA data are taken from [42].

Method	PS	fcc	hcp	bcc	sc	dia
KS–DFT	TM–NLPS	−57.207	0.038	0.106	0.400	0.819
		(−56.455)	(0.038)	(0.094)	(0.368)	(0.740)
KS–DFT	BLPS	−57.955	0.038	0.087	0.362	0.819
		(−57.153)	(0.035)	(0.080)	(0.353)	(0.749)
OF–DFT/WGC	BLPS	−57.941	0.018	0.079	0.354	0.827
		(−57.127)	(0.016)	(0.072)	(0.338)	(0.733)
OF–DFT/WT	BLPS	−57.940	0.020	0.080	0.330	0.851
		(−57.128)	(0.018)	(0.072)	(0.323)	(0.764)
OF–DFT/WGC[a]	BLPS	−57.954	0.018	0.094	0.308	0.828
		(−57.140)	(0.017)	(0.087)	(0.288)	(0.734)

[a]Modified WGC KEDF using $C_o = 0.25$ (see text).

Table 3. KS-DFT and OF-DFT calculations for elastic constants (GPa) of fcc Al using TM-NLPS/BLPSs, WGC/WT KEDFs within OF-DFT, and LDA/GGA XCs. GGA calculations are shown in parentheses. Experimental values are also listed.

Method	PS	C_{11}	C_{12}	C_{44}
KS-DFT	TM-NLPS	136.1 (120.6)	59.1 (54.3)	40.7 (35.6)
KS-DFT	BLPS	120.9 (109.1)	65.8 (63.3)	39.5 (37.6)
OF-DFT/WGC	BLPS	114.5 (104.5)	64.4 (60.9)	47.8 (44.6)
OF-DFT/WT	BLPS	110.3 (100.9)	72.7 (68.8)	32.6 (31.8)
OF-DFT/WGC[a]	BLPS	127.5 (114.8)	52.7 (50.1)	28.0 (26.6)
Experiment[b]		108.2	61.3	28.5

[a]Modified WGC KEDF using $C_o = 0.25$ (see text).
[b]Ref. [68].

of these two physical quantities. The shear modulus is directly related to the elastic constants of fcc Al; OF-DFT and KS-DFT values for these quantities are listed in Table 3. Neither KS-DFT nor OF-DFT perfectly reproduces the experimental elastic constants. OF-DFT/WT shows reasonable agreement with experimental data. However, because of the density-independent kernel, the WT KEDF is not reliable for systems in which the electron density varies rapidly, such as vacancies or surfaces [29,30], or more generally, any system with vacuum (e.g. isolated dislocation cores in periodic supercells). The WGC KEDF accurately reproduces C_{11} and C_{12}, but gives too high a value for C_{44} (47.8 and 44.6 GPa with LDA and GGA, respectively) compared to the experimental measurement of 28.5 GPa. This overestimation of C_{44} is also observed in the more accurate KS-DFT/TM-NLPS/LDA calculation (see Table 3).

The SFEs computed using OF-DFT and KS-DFT with various exchange-correlation functionals and pseudopotentials are displayed in Table 4 and the SFE curves are displayed in Figure 1. Within KS-DFT, the SFEs computed using the BLPS are 17–66 mJ m^{-2} smaller than those computed using the TM-NLPS with the LDA and GGA XCs. (Note that 66 mJ m^{-2} corresponds to 29 meV/atom, which is roughly within the expected accuracy of the physics contained within OF-DFT/WGC-KEDF for Al.) Although these energy differences are indeed quite small, the effect on the predicted dislocation width nevertheless could be non-negligible. Unfortunately, unlike KS-DFT, OF-DFT can only use LPSs that lack the requisite angular momentum dependence to better capture such small energy differences. Therefore, we must expect errors roughly of this magnitude as inevitable with the OF-DFT method. Lastly, inspection of the data in Table 4 reveals that the OF-DFT/BLPS calculations with the WGC and WT KEDFs produce even smaller SFEs (larger error with respect to KS-DFT/TM-NLPS) than KS-DFT/BLPS, with the WGC KEDF predictions closer to the KS-DFT results (as clearly illustrated in Figure 1).

To improve upon the aforementioned OF-DFT calculations of C_{44} and the SFEs, we must consider the two main sources of error in our calculations, namely the KEDF and the BLPS. Although refitting the BLPS to KS-DFT/NLPS beyond phase energy orderings would be an option to improve these properties, instead here we

Table 4. KS-DFT and OF-DFT calculations for stacking fault energies ($mJ\,m^{-2}$) in fcc Al (twinning energy γ_t, unstable stacking fault energy γ_{us}, intrinsic stacking fault energy γ_{isf}, unstable twinning energy γ_{ut}, extrinsic stacking fault energy γ_{esf}) using TM-NLPS/BLPSs, WGC/WT KEDFs within OF-DFT, and LDA/GGA XCs. GGA calculations are shown in parentheses. KS-DFT/TM-NLPS/LDA, KS-DFT/BLPS/LDA, and OF-DFT/WGC/BLPS/LDA data are taken from [42].

Method	PS	γ_t	γ_{us}	γ_{isf}	γ_{ut}	γ_{esf}
KS-DFT	TM-NLPS	57 (48)	188 (160)	140 (117)	254 (212)	149 (122)
KS-DFT	BLPS	40 (31)	143 (129)	93 (81)	188 (168)	105 (91)
OF-DFT/WGC	BLPS	32 (27)	139 (128)	67 (58)	171 (157)	64 (55)
OF-DFT/WT	BLPS	22 (18)	107 (97)	54 (45)	139 (124)	53 (44)
OF-DFT/WGC[a]	BLPS	46 (41)	157 (141)	92 (82)	197 (176)	92 (82)
Experiment		75[b]		135[b]		180[b]
		75[d]		150[c]		
		120[e]		166[d]		
				200[e]		

[a]Modified WGC KEDF using $C_o = 0.25$.
[b]Ref. [69].
[c]Ref. [70].
[d]Ref. [71].
[e]Ref. [72].

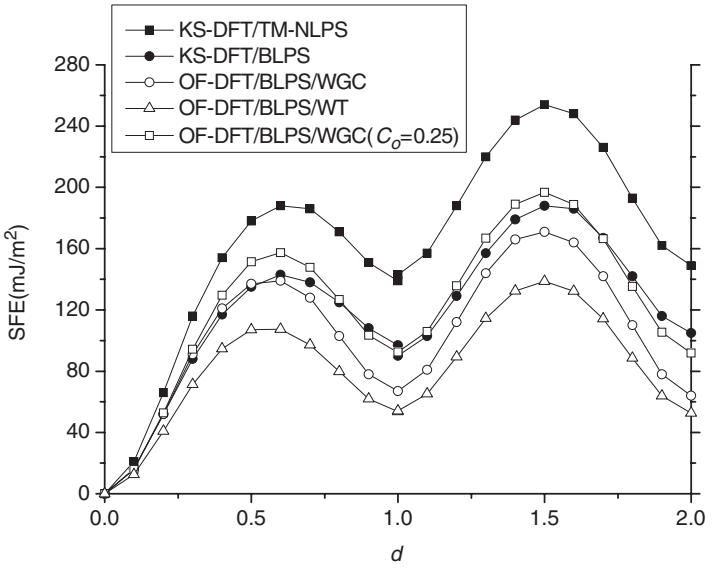

Figure 1. SFEs as a function of the fractional displacement d along the [112] direction calculated within the LDA. The translation is $\frac{a}{\sqrt{6}}d$, where a is the lattice constant of fcc Al. The curves are calculated with the setup (a) (from $d=0$ to $d=1$) and (b) (from $d=1$ to $d=2$) as given in Figure 3 of [66]. Only twin boundaries exist at $d=0$, which is taken to be the zero of the energy scale. (The twin energies are reported in Table 4.) The unstable stacking fault (us), the intrinsic stacking fault (isf), the unstable twin (ut) and the extrinsic stacking fault (esf) correspond to $d \approx 0.6$, $d \approx 1.0$, $d \approx 1.5$ and $d \approx 2.0$, respectively. KS-DFT/TM-NLPS, KS-DFT/BLPS and OF-DFT/BLPS/WGC data are taken from [42].

revisit the form of the WGC KEDF. As noted before, the WGC KEDF cannot be Taylor-expanded beyond second order, thus leaving limited room for systematic improvement. At first, other values of the one tunable parameter γ were explored, but such variations produced no improvement in C_{44} or the SFEs. Therefore, we attempted an *ad hoc* fix by modifying the weights of the second-order terms in the WGC kernel by rewriting the kernel as

$$\begin{aligned} w_{\alpha,\beta}(\xi_\gamma(\vec{r},\vec{r}')|\vec{r}-\vec{r}'|) = {} & w_{\alpha,\beta}(k_F^*|\vec{r}-\vec{r}'|) \\ & + \left.\frac{\partial w_{\alpha,\beta}(\xi_\gamma(\vec{r},\vec{r}')|\vec{r}-\vec{r}'|)}{\partial\rho(\vec{r})}\right|_{\rho_*}\theta(\vec{r}) + \left.\frac{\partial w_{\alpha,\beta}(\xi_\gamma(\vec{r},\vec{r}')|\vec{r}-\vec{r}'|)}{\partial\rho(\vec{r}')}\right|_{\rho_*}\theta(\vec{r}') \\ & + C_d\left\{\left.\frac{\partial^2 w_{\alpha,\beta}(\xi_\gamma(\vec{r},\vec{r}')|\vec{r}-\vec{r}'|)}{\partial\rho^2(\vec{r})}\right|_{\rho_*}\frac{\theta^2(\vec{r})}{2} + \left.\frac{\partial^2 w_{\alpha,\beta}(\xi_\gamma(\vec{r},\vec{r}')|\vec{r}-\vec{r}'|)}{\partial\rho^2(\vec{r}')}\right|_{\rho_*}\frac{\theta^2(\vec{r}')}{2}\right\} \\ & + C_o\left\{\left.\frac{\partial^2 w_{\alpha,\beta}(\xi_\gamma(\vec{r},\vec{r}')|\vec{r}-\vec{r}'|)}{\partial\rho(\vec{r})\partial\rho(\vec{r}')}\right|_{\rho_*}\theta(\vec{r})\theta(\vec{r}')\right\}, \end{aligned} \tag{13}$$

where C_d and C_o are to be treated as adjustable parameters. We emphasize that this parameterization does not have a sound mathematical basis and should simply be treated as a fitting procedure. However, such modification of the kernel does not change the basic linear response behavior, since we can see by inspection of Equation (13) that the relationship of Equation (4) from which the kernel is originally derived still holds (for $\rho(\vec{r}) = \rho_*$).

To determine optimal values for C_d and C_o, we examined elastic constants and SFEs as a function of these coefficients, which were allowed to vary from between 0 to 1.5, as illustrated in Figures 2 and 3. As seen from these figures, the elastic constants and SFEs are less sensitive to C_d and therefore we set its value to unity (as in the original Taylor expansion) to reduce the number of fitting parameters. Thereafter, we set $C_o = 0.25$ to obtain a value of C_{44} (see Figure 2 and Table 3) that is in excellent agreement with experiments, as well as SFEs that are in reasonable agreement with experimental and KS-DFT/BLPS results (see Figure 1 and Table 4). Lastly, note that this scaling of the off-diagonal second-order contribution to the WGC kernel also does not deleteriously affect the phase orderings in Al (see Table 2). Although OF-DFT is a first-principles method, use of this modified KEDF renders any simulations made using it semi-empirical. We examine next the influence of this modification of the WGC KEDF on dislocation width.

4.2. *OF-DFT simulations of dislocations in fcc Al*

We introduce $\langle 110\rangle/\{111\}$ screw and edge dislocations in quadrupolar and dipolar arrangements, respectively, as noted previously, using anisotropic linear elastic displacement fields [33]. To confirm that our results are independent of dislocation spacing, we also study isolated dislocations in large cylinders. As noted earlier, details of the various simulation cells are provided in Table 1. Upon electronic and ionic optimization, the dislocations spontaneously dissociate into two Shockley partials. The spacing between these partials (the dislocation width) is measured using the differential displacement approach [73] as indicated in Figure 4; since the

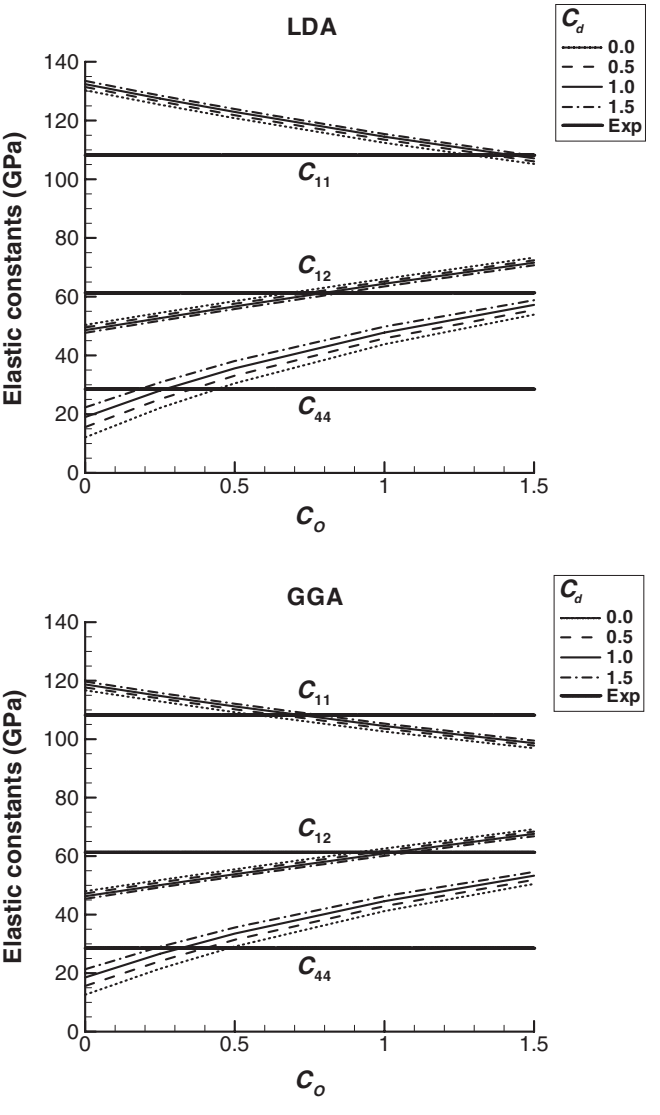

Figure 2. Elastic constants, C_{11}, C_{12} and C_{44}, as a function of the diagonal and off-diagonal coefficients in the second-order Taylor expansion of the WGC KEDF kernel [Equation (13)]. Experimental values [68] are indicated by the horizontal line.

dislocation core can only be localized up to the lattice spacing using this procedure, uncertainties of $\frac{\sqrt{6}}{4}a_0$ (2.5 Å) and $\frac{\sqrt{2}}{4}a_0$ (1.4 Å) (i.e. the lattice spacing along the $\langle 112 \rangle$ or $\langle 110 \rangle$ directions in Figure 4) must be expected for screw and edge dislocations, respectively.

In Table 5, we display the dislocation core width computed with OF-DFT using various KEDFs and XC functionals. For screw and edge dislocations in quadrupolar and dipolar arrangements, respectively, the modified WGC KEDF with LDA XC

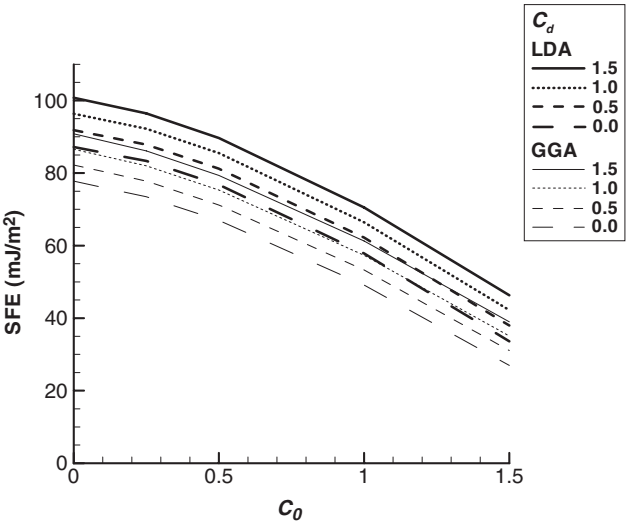

Figure 3. Intrinsic SFEs as a function of the diagonal and off-diagonal coefficients in the second-order Taylor expansion of the WGC KEDF kernel [Equation (13)].

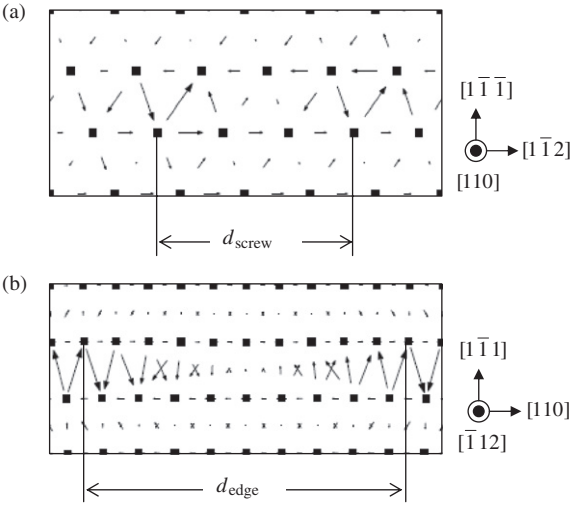

Figure 4. Differential displacement plots of OF-DFT optimized core structures for (a) screw and (b) edge components of dissociated screw and edge dislocations, respectively, using the modified WGC KEDF with the LDA XC. From the figures, we infer widths of 7.4 Å and 13.7 Å for the screw and edge dislocations, respectively. Squares indicate atom positions projected on the plane normal to the dislocation line, and arrows indicate differential displacements.

produces the smallest dislocation width, whereas the WT KEDF with GGA XC produces the largest width. This trend (width in inverse proportion to SFE) may be anticipated from the SFEs listed in Table 4. The dislocation width, as determined with the original and modified WGC KEDFs, is relatively insensitive to the type

Table 5. OF-DFT optimized separation distances (Å) between partials using BLPSs, WGC/WT KEDFs and LDA/GGA XCs. Quadrupole (screw) or dipole (edge) versus isolated single core unit cells are compared. GGA calculations are shown in parentheses.

Dislocation	Supercell	WGC	WT	WGC[a]
Screw	Quadrupole	10.7 (12.4)	11.6 (12.4)	7.4 (8.3)
	Isolated single core	10.7	8.3	5.8
Edge	Dipole	19.4 (23.7)	25.1 (26.5)	13.7 (17.3)
	Isolated single core	17.3	20.1	13.7

[a]Modified WGC KEDF using $C_o = 0.25$.

Table 6. Widths (Å) of screw and edge dislocations in fcc Al. Results from this work using the modified WGC KEDF ($C_o = 0.25$) and the LDA XC are compared with prior theoretical and experimental studies. The core width, determined in this work from differential displacement plots, has uncertainties of 2.5 Å and 1.4 Å for screw and edge dislocations, respectively.

Method	Screw	Edge
This work	7.4	13.7
FP-GFBC/GGA[a]	5.0–7.5	7.0–9.5
QC-DFT-EAM[b]	–	5.6
EAM[c]	4.9	–
EAM[d]	16.0	16.0
EAM[e]	–	5.0/15.0
Experiment[f]	–	8.0

[a]Nye tensor (5.0 and 7.0 Å) and differential displacement (7.5 and 9.5 Å) methods are used to identify the core positions in [40].
[b]Ref. [41].
[c]Ref. [37].
[d]Ref. [38] (Ercolessi–Adams potential [74]).
[e]Ref. [38] (Baskes et al. potential [75]).
[f]Ref. [34].

of simulation cell used (Table 5). This is not the case for the WT KEDF though, which shows appreciable differences in dislocation widths between the periodic and isolated cases. As noted before, we expect the WT KEDF to be less accurate for the isolated dislocation due to rapid variations in the charge density at the surface of the cylinder. In general, the modified WGC kernel, which captures SFEs and C_{44} more accurately, also produces dislocation widths that are in better agreement with KS-DFT and/or experiment than predictions from WGC or WT KEDFs, as we now discuss.

Our results are compared to results from prior computational studies and experiments in Table 6. There we see that our screw dislocation width is in excellent agreement with FP-GFBC predictions of Woodward et al. [40], which employ KS-DFT for the atoms closest to the core. The edge dislocation width is somewhat

overestimated in comparison with FP-GFBC predictions and experimental estimates, although the OF-DFT predictions fall within the rather large range of EAM predictions. Nevertheless, the overall agreement between our OF-DFT calculations and prior estimates is encouraging. It is worth noting that the OF-DFT method allows us to simulate dislocation structures without any additional overhead and inevitable sources of errors associated with patching different materials models within multiscale/multiphysics approaches. Therefore, once the accuracy and transferability of the KEDF and BLPS is ascertained, one is only concerned with determining the appropriate initial and boundary conditions. Furthermore, the method is sufficiently inexpensive to allow for simulation cells that are large enough to minimize unwanted dislocation interactions, or to isolate dislocations electrostatically from free surfaces.

5. Conclusions

In summary, we have studied the structures of dissociated screw and edge dislocations in fcc Al using OF-DFT. We have examined in detail the main sources of error in OF-DFT, namely the KEDF and the LPS, and ascertained their effects on the elastic moduli and SFEs of fcc Al. Through a slight modification of the WGC kernel in the KEDF, we have shown that the elastic moduli and SFEs can be brought into good agreement with KS-DFT and experimental estimates. As a consequence, dislocation widths are also found to be in good agreement with existing KS-DFT and experimental estimates in the literature.

The main advantage of the OF-DFT method is the ability to achieve first-principles accuracy for nearly-free-electron-like systems containing a large number (10^3–10^6) of atoms at relatively low computational cost [24,25]. This appealing feature makes OF-DFT a simulation tool that can bridge the gap between traditional KS-DFT, which is accurate but computationally expensive, and EAM potentials, which are less accurate but computationally inexpensive. The ability to simulate a large number of atoms directly implies that (a) calculations can be made free of internal boundaries that arise when patching regions in multiscale/multiphysics methods and that invariably are additional sources of inaccuracy, and (b) defects can be electrostatically isolated from external surfaces. Both of these issues are of great importance for accurate calculation of defect properties. There are, of course, some limitations of the OF-DFT method. Primary among these is the range of applicability of the method, which is limited at present to nearly-free-electron-like systems. This certainly precludes simulations of covalent and ionic systems, as well as metals with partially filled *d*-shells. Efforts are currently underway to extend the applicability of the method [76]. The search for accurate KEDFs also remains a problem of current research [77]. Finally, the computational cost, while much less than KS-DFT, is still sufficiently high to preclude long molecular dynamics trajectories or even multi-million atom molecular statics. As we commemorate 25 years of Finnis and Sinclair's seminal work [16], we foresee classical potential methods remaining the method of choice for such problems. Nevertheless, we are optimistic that OF-DFT is poised to become the method of choice for studying the energetics and kinetics of defects in main group metals.

Acknowledgements

We are grateful to the Office of Naval Research for funding this work and Princeton University for supercomputing time. L. Hung thanks the National Defense Science and Engineering Graduate Fellowship program. We also wish to thank Drs. Yue Qi and Louis Hector for suggesting this study.

References

[1] A. Ramasubramaniam and E.A. Carter, Mater. Res. Soc. Bull. 32 (2007) p.913.
[2] S.C. Glotzer and W. Paul, Annu. Rev. Mater. Res. 32 (2002) p.401.
[3] P. Hohenberg and W. Kohn, Phys. Rev. 136 (1964) p.B864.
[4] W. Kohn and L.J. Sham, Phys. Rev. 140 (1965) p.A1133.
[5] L.E. Ramos, J. Furthmüller, L.M.R. Scolfaro, J.R. Leite and F. Bechstedt, Phys. Rev. B 66 (2002) p.075209.
[6] D. Alfé, Phys. Rev. B 68 (2003) p.064423.
[7] N.D.M. Hine, P.D. Haynes, A.A. Mostofi, C.-K. Skylaris and M.C. Payne, Comput. Phys. Comm. 180 (2009) p.1041.
[8] F. Shimojo, R.K. Kalia, A. Nakano, K. Nomura and P. Vashishta, J. Phys. Condens. Matter 20 (2008) p.294204.
[9] A. Nakano, R.K. Kalia, K. Nomura, A. Sharma, P. Vashishta, F. Shimojo, A.C.T. van Duin, W.A. Goddard, R. Biswas, D. Srivastava and L.H. Yang, Int. J. High Perform. Comput. Appl. 22 (2008) p.113.
[10] F. Shimojo, R.K. Kalia, A. Nakano and P. Vashishta, Phys. Rev. B 77 (2008) p.085103.
[11] C.-K. Skylaris, P.D. Haynes, A.A. Mostofi and M.C. Payne, J. Chem. Phys. 122 (2005) p.084119.
[12] P.D. Haynes, C.-K. Skylaris, A.A. Mostofi and M.C. Payne, Phys. Status Solidi (b) 243 (2006) p.2489.
[13] J.M. Soler, E. Artacho, J.D. Gale, A. García, J. Junquera, P. Ordejón and D. Sánchez-Portal, J. Phys. Condens. Matter 14 (2002) p.2745.
[14] M.J. Gillan, D.R. Bowler, A.S. Torralba and T. Miyazaki, Comput. Phys. Comm. 177 (2007) p.14.
[15] J. VandeVondele, M. Krack, F. Mohamed, M. Parrinello, T. Chassaing and J. Hutter, Comput. Phys. Comm. 167 (2005) p.103.
[16] M.W. Finnis and J.E. Sinclair, Phil. Mag. A 50 (1984) p.45.
[17] M.S. Daw and M.I. Baskes, Phys. Rev. Lett. 50 (1983) p.1285.
[18] M.S. Daw and M.I. Baskes, Phys. Rev. B 29 (1984) p.6443.
[19] K.M. Carling and E.A. Carter, Model. Simulat. Mater. Sci. Eng. 11 (2003) p.339.
[20] G. Ho, C. Huang and E.A. Carter, Curr. Opin. Solid State Mater. Sci. 11 (2008) p.57.
[21] G. Ho, M.T. Ong, K.J. Caspersen and E.A. Carter, Phys. Chem. Chem. Phys. 9 (2007) p.4951.
[22] B.J. Jesson and P.A. Madden, J. Chem. Phys. 113 (2000) p.5924.
[23] E. Smargiassi and P.A. Madden, Phys. Rev. B 49 (1994) p.5220.
[24] G.S. Ho, V.L. Ligneres and E.A. Carter, Comput. Phys. Comm. 179 (2008) p.839.
[25] L. Hung and E.A. Carter, Chem. Phys. Lett. 475 (2009) p.163.
[26] T. Darden, D. York and L. Pedersen, J. Chem. Phys. 98 (1993) p.10089.
[27] U. Essmann, L. Perera, M. Berkowitz, T. Darden, H. Lee and L.G. Pedersen, J. Chem. Phys. 103 (1995) p.8577.
[28] N. Choly and E. Kaxiras, Phys. Rev. B 67 (2003) p.155101.
[29] Y.A. Wang, N. Govind and E.A. Carter, Phys. Rev. B 60 (1999) p.16350.
[30] Y.A. Wang, N. Govind and E.A. Carter, Phys. Rev. B 64 (E) (2001) p.089903.

[31] L.-W. Wang and M.P. Teter, Phys. Rev. B 45 (1992) p.13196.
[32] M. Foley and P.A. Madden, Phys. Rev. B 53 (1996) p.10589.
[33] J.P. Hirth and J. Lothe, *Theory of Dislocations*, 2nd ed., John Wiley & Sons, New York, 1982.
[34] W. Höllerbauer and H.P. Karnthaler, Beitr. Elektronenmikroskop. Direktabb. Oberfl. 14 (1981) p.361.
[35] X.Z. Liao, F. Zhou, E.J. Lavernia, S.G. Srinivasan, M.I. Baskes, D.W. He and Y.T. Zhu, Appl. Phys. Lett. 83 (2003) p.632.
[36] X.Z. Liao, S.G. Srinivasan, Y.H. Zhao, M.I. Baskes, Y.T. Zhu, F. Zhou, E.J. Lavernia and H.F. Xu, Appl. Phys. Lett. 84 (2004) p.3564.
[37] V.V. Bulatov, O. Richmond and M.V. Glazov, Acta Mater. 47 (1999) p.3507.
[38] S.G. Srinivasan, X.Z. Liao, M.I. Baskes, R.J. McCabe, Y.H. Zhao and Y.T. Zhu, Phys. Rev. Lett. 94 (2005) p.125502.
[39] C. Woodward and S. Rao, Phys. Rev. Lett. 88 (2002) p.216402.
[40] C. Woodward, D.R. Trinkle, L.G. Hector Jr. and D.L. Olmsted, Phys. Rev. Lett. 100 (2008) p.045507.
[41] G. Lu, E.B. Tadmor and E. Kaxiras, Phys. Rev. B 73 (2006) p.024108.
[42] C. Huang and E.A. Carter, Phys. Chem. Chem. Phys. 10 (2008) p.7109.
[43] J. Lindhard, Kgl. Danske Videnskab. Selskab Mat.-Fys. Medd. 28 (1954) p.8.
[44] L.H. Thomas, Proc. Cambridge Phil. Soc. 23 (1927) p.542.
[45] E. Fermi, Rend. Accad. Naz. Lincei 6 (1927) p.602.
[46] E. Fermi, Z. Phys. 48 (1928) p.73.
[47] C.F. von Weizsäcker, Z. Phys. 96 (1935) p.431.
[48] E. Teller, Rev. Mod. Phys. 34 (1962) p.627.
[49] J.C. Slater and H.M. Krutter, Phys. Rev. A 47 (1935) p.559.
[50] M. Pearson, E. Smargiassi and P.A. Madden, J. Phys. Condens. Matter 5 (1993) p.3321.
[51] F. Perrot, J. Phys. Condens. Matter 6 (1994) p.431.
[52] M. Foley, E. Smargiassi and P.A. Madden, J. Phys. Condens. Matter 6 (1994) p.5231.
[53] E. Smargiassi and P.A. Madden, Phys. Rev. B 51 (1995) p.117.
[54] B.J. Jesson, M. Foley and P.A. Madden, Phys. Rev. B 55 (1997) p.4941.
[55] Y.A. Wang, N. Govind and E.A. Carter, Phys. Rev. B 58 (1998) p.13465.
[56] Y.A. Wang, N. Govind and E.A. Carter, Phys. Rev. B 64(E) (2001) p.129901.
[57] G. Ho, V.L. Ligneres and E.A. Carter, Phys. Rev. B 78 (2008) p.045105.
[58] B. Zhou, Y.A. Wang and E.A. Carter, Phys. Rev. B 69 (2004) p.125109.
[59] X. Gonze, J.-M. Beuken, R. Caracas, F. Detraux, M. Fuchs, G.-M. Rignanese, L. Sindic, M. Verstraete, G. Zerah, F. Jollet, M. Torrent, A. Roy, M. Mikami, P. Ghosez, J.-Y. Raty and D.C. Allan, Comput. Mater. Sci. 25 (2002) p.478.
[60] D.M. Ceperley and B.J. Alder, Phys. Rev. Lett. 45 (1980) p.566.
[61] J.P. Perdew and A. Zunger, Phys. Rev. B 23 (1981) p.5048.
[62] J.P. Perdew, K. Burke and M. Ernzerhof, Phys. Rev. Lett. 77 (1996) p.3865.
[63] N. Troullier and J.L. Martins, Phys. Rev. B 43 (1991) p.1993.
[64] J. Nocedal and S.J. Wright, *Numerical Optimization*, Springer, New York, 1999.
[65] W.H. Press, B.F. Flannery, S.A. Teukolsky and W.T. Vetterling, *Numerical Recipes: The Art of Scientific Computing*, Cambridge University Press, Cambridge, 1986.
[66] N. Bernstein and E.B. Tadmor, Phys. Rev. B 69 (2004) p.094116.
[67] J.R.K. Bigger, D.A. McInnes, A.P. Sutton, M.C. Payne, I. Stich, R.D. King-Smith, D.M. Bird and L.J. Clarke, Phys. Rev. Lett. 69 (1992) p.2224.
[68] H.B. Huntington, Solid State Phys. 7 (1958) p.213.
[69] R.E. Smallman and P.S. Dobson, Metall. Trans. 1 (1970) p.2383.
[70] M.J. Mills and P. Stadelmann, Phil. Mag. A 60 (1989) p.355.

[71] L.E. Murr, *Interfacial Phenomena in Metals and Alloys*, Addison Wesley, Reading, MA, 1975.
[72] I.L. Dillamore and R.E. Smallman, Phil. Mag. 12 (1965) p.191.
[73] V. Vitek, R.C. Perrin and D.K. Bowen, Phil. Mag. 21 (1970) p.1049.
[74] F. Ercolessi and J.B. Adams, Europhys. Lett. 26 (1995) p.583.
[75] M.I. Baskes, J.E. Angelo and N.R. Moody, in *Hydrogen Effects in Materials*, A.W. Thompson and N.R. Moody, eds., The Minerals, Metals and Materials Society, Warrendale, PA, 1996, p.77.
[76] C. Huang and E.A. Carter, to be published.
[77] Y.A. Wang and E.A. Carter, *Orbital-free kinetic energy density functional theory*, in *Theoretical Methods in Condensed Phase Chemistry*, Chap. 5, Kluwer, Dordrecht, 2000, p.117.